Using evolutionary algorithms to design antennas with greater sensitivity to ultrahigh energy neutrinos

J. Rolla[1,2,*] A. Machtay,[1] A. Patton,[1] W. Banzhaf,[3] A. Connolly,[1,†] R. Debolt,[1] L. Deer,[1] E. Fahimi,[1]
E. Ferstle,[1] P. Kuzma,[1] C. Pfendner,[4] B. Sipe,[1] K. Staats,[5] and S. A. Wissel[6]

(GENETIS Collaboration)

[1]*Department of Physics, Center for Cosmology and AstroParticle Physics, The Ohio State University, Columbus, Ohio 43210, USA*
[2]*Jet Propulsion Laboratory, NASA, Pasadena, California 91109, USA*
[3]*Department of Computer Science and Engineering, Michigan State University, East Lansing, Michigan 48824, USA*
[4]*Department of Physics and Astronomy, Denison University, Granville, Ohio 43023, USA*
[5]*University of Arizona, Biosphere 2, South Biosphere Road, Oracle, Arizona 85623, USA*
[6]*Department of Physics, Department of Astronomy and Astrophysics, Pennsylvania State University, State College, Pennsylvania 16802, USA*

The Genetically Evolved NEutrino Telescopes for Improved Sensitivity project seeks to optimize detectors in physics for science outcomes in high-dimensional parameter spaces. In this project, we designed an antenna using a genetic algorithm with a science outcome directly as the sole figure of merit. This paper presents initial results on the improvement of an antenna design for in-ice neutrino detectors using the current Askaryan Radio Array (ARA) experiment as a baseline. By optimizing for the effective volume using the evolved antenna design in ARA, we improve upon ARA's simulated sensitivity to ultrahigh energy neutrinos by 11%, despite using limited parameters in this initial investigation. Future improvements will continue to increase the computational efficiency of the genetic algorithm and the complexity and fitness of the antenna designs. This work lays the foundation for continued research and development of methods to increase the sensitivity of detectors in physics and other fields in parameter spaces of high dimensionality.

I. INTRODUCTION

The high-dimensional parameter spaces of detector design problems motivate using a heuristic to improve upon designs made using traditional techniques. A heuristic is a computational method for efficiently finding a high-quality solution to a given problem without evaluating all possible solutions. In particular, the design of antennas for ultrahigh energy (UHE) neutrino detection has explicit constraints and a high-dimensional parameter space, making it well suited for heuristic optimization. Given the immense scale of these experiments and the low flux of UHE neutrinos, each detector element must be designed to return the best science outcome for its cost.

The Genetically Evolved NEutrino Telescopes for Improved Sensitivity (GENETIS) project aims to optimize the science outcomes of detector designs in high-dimensional parameter spaces to advance the field of physics. As a first application, GENETIS has produced a genetic algorithm (GA) [1] that evolves antenna geometries optimized for UHE neutrino detection in a six-dimensional parameter space. GENETIS applies a heuristic optimization method for designing an antenna using a *science outcome* as the sole measure of fitness.

This paper presents initial results from GENETIS on the improvement of antenna designs used in UHE neutrino experiments with a limited number of parameters. This study aims to provide a proof of concept for using GAs to optimize detectors for science outcomes.

GENETIS chose to use GAs, among other potential computational intelligence and machine learning algorithms, for antenna design because of their effectiveness at complex optimization problems, especially when many

[*]julie.a.rolla@jpl.nasa.gov
Present address: Jet Propulsion Laboratory, NASA, Pasadena, California 91109, USA.
[†]connolly@physics.osu.edu

optima could exist [2]. GAs are also often more transparent than other methods, such as machine learning optimization techniques, which allows for an intuitive understanding of how the algorithm arrived at a final result. Searching the six-dimensional parameter space explored in this investigation using increments of the size necessary to find a peak fitness score would require the evaluation of more than 10^8 designs. By contrast, the GA used here needed only 1550 designs to search the parameter space.

The use of GAs was initially motivated by the NASA ST-5 antenna, in which a GA designed a simple segmented wire antenna for satellite communications [3]. Many other examples of antenna design optimization using GAs exist, including Yagi-Uda antennas [4], electrically loaded wire antennas [5], broadband cage antennas [6], planar antennas [7], pyramid horn antennas [8], ultrawideband slot antennas [9], helical antennas [10], patch antennas [11], adaptive antennas [12,13], and others [14].

GAs have previously been used in the design of various detectors and experiments, although rarely to optimize for a science outcome directly [15,16]. A horn antenna was designed using a GA optimized for the detection of cosmic microwave background radiation [17]. Both the Long-Baseline Neutrino Oscillation experiment and the Deep Underground Neutrino Experiment employed GAs to optimize the design of neutrino beamlines using simulations of a science outcome to determine the fitness [18,19]. GAs have also been used to optimize the layout of detectors, sensors, shielding, and trigger optimization [20–24].

Here, we report on the initial evolution of bicone antennas for use in radio UHE neutrino detection experiments. Using the simulated sensitivity of the antennas to neutrino interactions as the fitness score, we evolved antennas that exceed the performance of antennas now in service. This paper begins with a brief background discussion of GAs and UHE neutrino detection. Next, a description of the antenna geometry used and the associated constraints is given in Sec. IV. In Sec. V, the GENETIS GA is presented in detail. Next, the results and subsequent discussion are presented. Finally, the conclusion and future steps of the GENETIS project are given. Appendix A provides the derivation of a single frequency matching circuit. Appendix B discusses the steps taken to investigate and optimize the parameters of the GA. Additional gain patterns are provide in Appendix C to supplement those in Sec. VI. An evolution of a symmetric biconical antenna is given in Appendix D for comparison to the results of this paper.

II. GENETIC ALGORITHMS

A GA is an optimization technique that applies natural selection to generate populations of individuals so that they evolve toward an improved outcome [25–34]. Individuals are defined solely by their genes, which are a set of values representing the individual's characteristics. These genes form the parameter space that the GA explores. The population of individuals makes up a group of potential solutions to the problem. An individual is assessed based on its fitness score, which is the objective score that the algorithm is designed to maximize. This fitness score is the criterion used by the GA to select individuals to pass their genes to the next generation. For example, a GA may be used to optimize for the largest volume of a box-shaped container given a constant surface area. The fitness score would then be the volume of the box, which becomes higher as the box evolves into a cube.

Each new generation of individuals is created by first selecting individuals from the prior generation to form the new individuals. These "selection methods" are probabilistic in nature, incorporating the fitness score of the individuals to promote the selection of better performing individuals. After individuals are selected, modifications are performed on their genes to form the new individuals that populate the next generation. These techniques are called genetic operators [35] and are discussed in detail in Sec. V C.

III. UHE NEUTRINOS

One important missing piece of particle astrophysics is the detection of UHE neutrinos with energies above about 10^{17} eV [36]. Neutrinos do not carry an electric charge and are weakly interacting, which means they can be traced back to their source more readily than other cosmic particles. However, the properties that make neutrinos resilient communicators also make them extremely difficult to detect. Their low flux of approximately tens of UHE neutrinos per km^2 per year per steradian [37–40], and their interaction lengths of order 1000 km in the earth [41,42] necessitates that experiments view on the order of ~ 100 km^3 to detect a single UHE neutrino in a year.

Many experiments are employing antenna arrays to detect Askaryan radiation produced when a neutrino collides within a large dielectric volume (such as ice in Antarctica or Greenland) [43,44]. The resulting shower moves through the ice faster than the speed of light (in ice), creating a cone of Askaryan radiation. These experiments include ANITA and PUEO, ARA, ARIANNA, and RNO-G, which use a variety of different antenna types [40,45–49]. Differing from optical-Cherenkov experiments such as IceCube, Askaryan-focused experiments seek to explore higher energies, currently with best constraints above $10^{19.5}$ eV.

ARA is located at the South Pole, a few kilometers from the IceCube Neutrino Observatory. It consists of five stations buried in the Antarctic: one prototype station 100m deep and four stations 200 m deep [50]. Each station consists of four measurement strings, which consist of two vertically polarized antennas and two horizontally polarized antennas, for a total of 16 antennas per station. The measurement strings are located approximately 20 m apart, forming a square [50–52].

ARA uses two different antenna designs to detect vertically polarized (Vpol) signals and horizontally polarized (Hpol) signals. ARA antennas must be designed to fit

in narrow holes drilled in the ice. The ARA antennas are broadband, with the Vpol antennas being birdcage bicones (13.9 cm diameter) with bandwidth 150–850 MHz, while the Hpol antennas are ferrite-loaded quad-slot antennas (12.7 cm diameter), with bandwidth 200–850 MHz [50–52]. This work uses ARA as a test case, evaluating antenna performance with ARA simulation software and comparing the evolved designs to the ARA Vpol antennas.

IV. THE ASYMMETRIC BICONE ANTENNA

The results presented in this paper involve the evolution of an asymmetric bicone antenna, as illustrated in Fig. 1. A bicone antenna consists of two cones with openings facing opposite directions. This shape was chosen because it is similar to antennas currently deployed in the ARA experiment and has a broadband response, which is desirable for the detection of the broadband Askaryan emission. The asymmetric bicone used here is entirely defined by six genes (parameters): the inner radius (r), the length (L), and the opening angle (θ) for the top and bottom cones. A single individual in the GA is an antenna design given by these six parameters.

An asymmetric design was chosen for this work because the additional genes give a larger parameter space to explore than a symmetric design. In the interest of comparison, an evolution of symmetric antennas was conducted and is shown in Appendix D.

The GA constrains the diameter of the antennas to 15 cm to match the diameter of the ARA boreholes [53]. The outer diameter of the antenna is therefore prevented from being larger than the ARA borehole width (both during initialization and in later generations). While no required borehole diameter clearance (the distance between the antenna and the borehole) was specified in the GA, ARA uses a
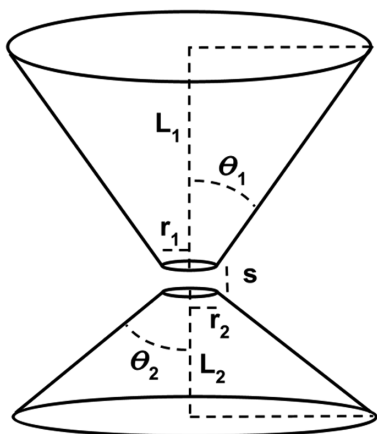
borehole clearance of 1.1 cm for the Vpol antennas and 2.3 cm for the HPol antennas [51]. Future experiments may drill larger boreholes (over 28 cm in diameter) [54]. This would improve antenna sensitivities since larger and more complex designs could be created (from the perspective of the GA, there would be a greater parameter space to explore). Here, we maintain the same borehole diameter that ARA currently uses to directly compare to ARA's Vpol antenna design.

In this initial investigation, the GA also constrains the minimum full length to be 75 cm (37.5 cm for each cone). Note that this requirement does not allow for the length of the current ARA bicone antennas, which have a full length of 50 cm. The length parameter space explored corresponds to dipole antenna resonance at frequencies lower than the usual frequency range considered for ARA, although biconical antennas operate in a wider band than their resonance. Future work will decrease this minimum length to 10 cm to fully explore the parameter space.

V. THE GENETIC ALGORITHM

Figure 2 presents a schematic of the GENETIS algorithm. An initial population is generated, and this begins an iterative cycle where a new generation is produced by selecting individuals from the prior generation and using variants of those individuals' genes to form the next generation. The process repeats until predetermined termination requirements are met. The following sections describe the GENETIS GA in more detail.

A. Initialization

The first population is initialized by selecting values for the six genes for each individual from a uniform distribution with a mean similar to the current ARA design. The parameters for the initialization can be seen in Table I. The aforementioned simulation constraint gives the minimum length. Using the minimum radius and length, the maximum angle is calculated as the angle that will cause the antenna width to equal the borehole diameter.

B. Fitness calculation

Once every individual in a generation is defined, the fitness score of each individual must be determined. The

FIG. 1. A schematic of an asymmetric bicone antenna. The lengths (L_1, L_2), inner radii (r_1, r_2), opening angles (θ_1, θ_2), and separation distance (s) fully define the geometry. In the results presented here, the separation distance was held constant, and the other six parameters were varied.
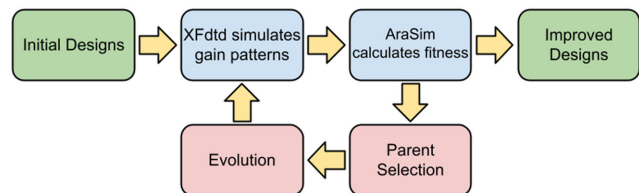

FIG. 2. A diagram of the GENETIS work flow used to evolve antennas. The boxes on the far left and right give the beginning and end of the loop. The two central boxes represent the fitness calculation and the bottom two boxes represent the creation of the next generation.

TABLE I. Range of uniform distributions used for each gene.

Gene	Minimum	Maximum
Length (cm)	37.5	140
Radius (cm)	0.0	7.5
Opening angle (degrees)	0.0	11.3

fitness score is a measure of performance evaluated for each individual in a generation and is used by the tournament and roulette methods (see Sec. V C). A higher fitness score indicates that the individual performed better. The calculation of fitness scores is a multistep process that involves two main programs integrated with the GA. First, the gain pattern of each individual is simulated. Then, a measure of the ARA detector's sensitivity to neutrino-induced radio signals is calculated by running a neutrino detection simulation software using the individual for the Vpol antennas. This measure of sensitivity is the final fitness score.

The first step in evaluating the fitness of an individual is to model its geometry in XFdtd, a commercial electromagnetic simulation software by Remcom [55]. XFdtd simulates the antenna response at 60 different frequencies (equal steps from approximately 100 to 1000 MHz) at each azimuth-zenith coordinate (in steps of 5°). An antenna's gain is a measure of how efficiently it converts received radio waves from a given direction into power. XFdtd calculates the far-zone absolute gain (hereafter referred to as simply "gain") of an antenna at a specific (θ, ϕ) coordinate using Eq. (1) [56]:

$$G = \frac{2\pi r^2 |\tilde{E}(\theta, \phi)|^2}{\eta P_0}. \tag{1}$$

Here, G is the absolute far-zone gain [57] of the antenna in a specific direction, which XFdtd reports in dBi. $\tilde{E}(\theta, \phi)$ gives the complex electric field incident on the antenna from the (θ, ϕ) direction, η is the wave impedance in the medium (377 Ω in free space), r is the distance between the power source and the sensors in the simulation (1 m), and P_0 is the power accepted by the antenna. Antenna gain is related to the antenna's effective area by [58]

$$G = \frac{4\pi}{\lambda^2} A_e. \tag{2}$$

Note that Eqs. (1) and (2) are *not* the fitness score that will be used to evaluate an individual antenna's performance.

For the second step in calculating the fitness score, a neutrino detection simulation program called AraSim is used to measure the performance of the antenna [39]. Developed by the ARA Collaboration, AraSim can model neutrinos with energies between $E_\nu = 10^{17}$–10^{21} eV [39]. AraSim simulates high-energy neutrino interactions in the Antarctic ice that produce electromagnetic and hadronic

showers resulting in the production of Askaryan radiation. AraSim uniformly distributes these interactions within a cylindrical volume with a 3 km radius centered around the detector [39]. The direction of the incoming neutrino is uniformly distributed over a solid angle of 4π. The radio emission propagation is modeled using ray tracing, which determines the path length from the interaction to the detector. The ray tracing models the depth-dependent index of refraction of the ice, which is $n = 1.3$ at the surface to $n = 1.8$ at 200 m deep [39]. The simulation includes both the direct and refracted ray solutions [59]. Because of this variable index of refraction, the electromagnetic waves emitted from the interaction bend en route from the interaction point to the antenna. AraSim then calculates the polarization, viewing angle, and travel time at the receivers, and then models the system electronics, noise waveforms, and time-domain trigger [39].

GENETIS determines an individual's fitness score with AraSim by setting the response of the Vpol antennas to the individual's response generated by XFdtd for each of the 60 frequencies simulated. The sensitivity produced by AraSim, known as the effective volume, is used as the individual antenna's fitness score. The effective volume is a common quantity used to assess detector sensitivities in neutrino detection experiments making it a natural and convenient metric for antenna performance. Since the effective volume is directly proportional to the number of neutrinos detected, we can directly use it as the fitness score. The effective volume $[V\Omega]_{\text{eff}}$ is given by [37]

$$\text{Fitness Score} = [V\Omega]_{\text{eff}} = 4\pi V_{\text{ice}} \frac{N_{\text{detected}}}{N_{\text{simulated}}}, \tag{3}$$

where V_{ice} is the total volume of ice simulated in AraSim, N_{detected} is the total number of neutrinos detected, and $N_{\text{simulated}}$ is the total number of neutrinos simulated. In this analysis, V_{ice} is given by a cylinder around the detector with a radius of 3 km and a total volume of approximately 85 km^3. For each individual, $N_{\text{simulated}}$ is 3×10^5 neutrinos with an energy of 10^{18} eV. This energy was chosen because it is in the region of energies where ARA is expected to be most sensitive, as shown in Fig. 31 of [47]. Simulating this number of neutrinos gives a standard deviation of 0.2 km^3 sr in the effective volume.

The calculation of the fitness scores is a computationally heavy process and is conducted using cluster computing at the Ohio Supercomputing Center. The process is parallelized to spread $N_{\text{simulated}}$ across 10 different jobs for each individual, allowing each job to be completed in approximately six hours. Because of limitations on concurrently running jobs, the fitness score calculation takes 12 hours in total per generation when evolving 50 individuals per generation and generating 3×10^5 neutrinos per individual.

C. New generation creation

Roulette and tournament were the selection methods used in this GA. Roulette selection, also known as fitness proportionate selection, is where the probability of an individual being selected as a parent for the new generation is proportional to their fitness score [60]. In tournament selection, a subset of individuals is selected, and the one with the highest fitness score is selected as a parent [29,61].

Three genetic operators were then used: reproduction, injection, and uniform crossover. Reproduction uses a selection method to obtain one parent and passes that individual directly to the next generation. The injection operator generates entirely new individuals that are not derived from any parents. Uniform crossover takes two parents from the prior generation and generates a child whose genes each have a fifty percent chance of coming from each parent [62].

The proportions of individuals for which each of the selection methods and genetic operators were used were found through an optimization analysis. Different combinations of selection methods and genetic operators were tested through an exercise where an asymmetric bicone with the same six parameters as used here evolved to a predetermined geometry. The results presented here use the GENETIS algorithm with 50 individuals over 31 generations. For each new generation, 80% of parents were selected using roulette selection, and 20% were chosen through tournament selection. Four individuals competed in each tournament (the optimization analysis determined that it should be 7% of the population). The new population was generated using 72% crossover, 22% injection, and 6% reproduction.

D. Loop and termination

After the second generation is created, the GA continues to iterate and evolve individuals towards more optimal solutions. The loop was allowed to continue to run until it appeared that the growth in the average fitness score had plateaued and was terminated at generation 31. Tests using the optimization analysis have shown that the majority of growth should occur by approximately the 30th generation, so a plateaued mean around generation 30 indicates that there is little or no growth remaining.

VI. RESULTS

A. Results from evolution

The results of the evolution are presented in the violin plot in Fig. 3 showing clear evolution toward improved solutions. For each generation, the range of fitness scores is illustrated by the height of the violin. The top point of each generation shows the highest fitness score of that generation. The width of each violin represents the density of individuals with that score. The solid orange line shows the mean of the population, with the standard deviation on the
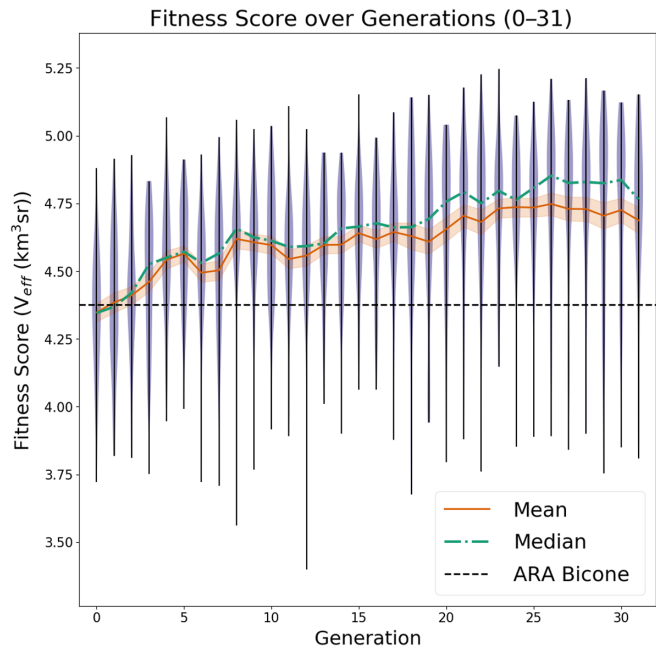

FIG. 3.   Initial results of GA. Each distribution represents the entire range of scores in the generation, while width indicates the density of scores. The current ARA Bicone Fitness is shown as the horizontal dotted line.

mean represented by the orange shading, and the dashed green line shows the median, which is useful for understanding the convergence of the population. Lower-scoring individuals are still present throughout the entire evolution, despite the average and maximum fitness scores improving beyond the initial generation. This is primarily due to the injection operator, which continually introduces new diversity to the population to prevent early convergence to local maxima [63]. The fitness scores used in the loop have an error of approximately 0.2 km^3 sr, which comes from the statistical uncertainties on the results from the AraSim Monte Carlo simulation.

The best performing individual found during the evolution was individual 8 from generation 23, with a fitness score of 5.25 ± 0.2 km^3 sr. After the conclusion of the evolution run, we assessed the top five best performing individuals with improved statistics. With a factor of 10 increase in the number of neutrinos simulated, the best performing individual remained the best performing individual within uncertainties, with a fitness score of 4.95 ± 0.04. To more accurately measure the improvement of the individual's performance over ARA's existing bicone antenna, we resimulated the highest scoring individual with a factor of 100 more neutrinos in AraSim. The best individual from the evolution produced a fitness score of 4.90 ± 0.1 km^3 sr, while the ARA bicone produced a score of 4.38 ± 0.02 km^3 sr. This represents an 11% improvement over the current Vpol design.

Figure 4 is a parallel coordinate plot that illustrates the genes and fitness scores of each individual in the evolution.
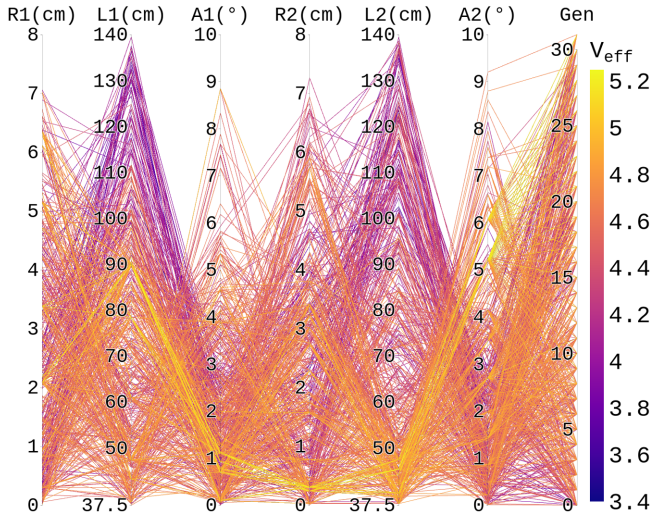
FIG. 4. Evolution of the six antenna parameters optimized so far, showing trends toward preferred features (bright yellow being most fit).

An individual is represented by a jagged line spanning the width of the plot, with the value of each of the individual's genes represented by the line's height on the vertical axes. The color of the line represents the individual's fitness score. The collection of yellow lines following a common path demonstrates the effectiveness of the GA at converging in later generations to higher-scoring individuals with similar design parameters.

Figure 4 also shows general trends in each of the genes and their impact on the fitness score. For example, most high scoring antennas share similar values, with the opening angles of the top cone (A1) being under 1 degree, the length of the bottom cone (L2) being less than 50 cm, and the angle of the bottom cone (A2) being between 4 and 6 degrees for high scoring antennas. However, the other parameters have a larger spread in viable values, with the radius of the top cone (R1) being spread across the entire parameter space for high-scoring individuals. The fitness score was not expected to depend highly on the inner radii because even the largest permitted radius was still smaller than any of the wavelengths simulated.

Figure 5 shows a three-dimensional (3D) model of the highest performing antenna evolved in this work. Notice that the top cone of the antenna is longer than the bottom, has a larger inner radius, and has a smaller opening angle.

FIG. 5. Model of the best antenna design, individual 8, evolved in generation 23. This bicone is shown on its side here, with the top side on the left. Other individuals are not shown because they are not visually distinguishable from this one.

TABLE II. Genes and fitness scores of the top five individuals from this evolution.

Cone	R1, R2 (cm)	L1, L2 (cm)	A1, A2 (rad)	Score (km^3 sr)
Top	**2.1**	**90.0**	**0.016**	**4.90 ± 0.01**
Bottom	**0.30**	**45.4**	**0.091**	
Top	2.1	90.0	0.016	4.93 ± 0.04
Bottom	0.30	45.4	0.091	
Top	2.1	90.0	0.020	4.91 ± 0.04
Bottom	0.30	45.4	0.091	
Top	2.1	90.0	0.020	4.91 ± 0.04
Bottom	0.24	45.4	0.091	
Top	2.1	90.0	0.020	4.78 ± 0.04
Bottom	0.24	45.4	0.091	

This is also true of the next best antennas, which had similar genes to the highest performing individual. Of the five highest scoring antennas, only a combined three genes (out of thirty) were more than 5% different from the highest scoring individual.

The genes and fitness score of the top individual are represented as the top bold row in Table II, along with the genes and fitness scores of the next top four performing individuals. The fitness scores listed in Table II are from re-simulation using 3×10^7 neutrinos for the top individual, and 3×10^6 neutrinos for the other four.

B. Comparing gain and realized gain

As discussed in Sec. V B, an antenna's gain is calculated in XFdtd using Eq. (1). While the antenna gain is not the fitness score, AraSim uses it to evaluate the fitness score. In addition to calculating the antenna gain that assumes perfect matching, XFdtd also calculates the *realized gain*. Realized gain accounts for the reflection of a received signal due to an impedance mismatch [57]. The results in Sec. VI B were generated using the gain assuming perfect matching. The reflection coefficient affects the power that reaches the antenna P_0. Given a power P_M reaching the matched transmission line, we have [58]

$$P_0 = P_M(1 - \Gamma^2), \qquad (4)$$

where Γ is the reflection coefficient. Minimal reflection occurs when the load and characteristic impedances are equal, as the reflection coefficient, given by

$$\Gamma = \frac{Z_a - Z_0}{Z_a + Z_0}, \qquad (5)$$

which is minimized when $Z_a = Z_0$. The realized gain G_R in XFdtd is given by the following equation, which replaces P_0 from Eq. (1) with P_M:
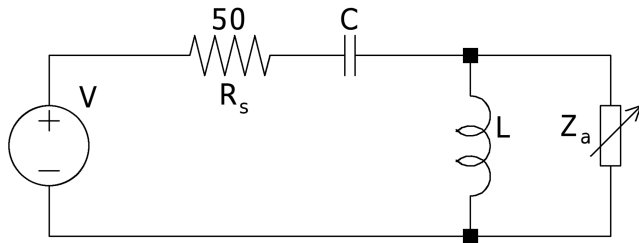
FIG. 6.   SPICE schematic of the matching circuit.

$$G_{\mathrm{R}} = \frac{2\pi r^2 |\tilde{E}(\theta, \phi)|^2}{\eta P_{\mathrm{M}}}. \tag{6}$$

For this work, a simple matching circuit was designed to match the impedance of the load to the source at 200 MHz, as shown in the Simulation Program with Integrated Circuit Emphasis (SPICE) schematic in Fig. 6 [64]. For the neutrino energy used in this work, the maximum power of the induced Askaryan radio signal occurs near 300 MHz for hadronic showers and 100 MHz for electromagnetic showers for events viewed within about 5 degrees of the Cherenkov angle [65]. The matching frequency was chosen to be 200 MHz because it is the frequency at which the ARA signal chain has maximal sensitivity for a typical Vpol receiving antenna [47].

Figure 6 is a schematic of a matching circuit for a radiating antenna at a single frequency. It is important to note that we are designing receiver antennas, but the schematic in Fig. 6 is for a transmitting antenna. This is because the antennas were modeled as transmitting antennas in XFdtd. When we build antennas produced from the GENETIS GA, we will use matching circuits that we will design for receiver antennas where the antenna takes the place of the source V and resistance R_s. The antenna impedance is matched to the radiating source V, which had an amplitude of 1 V, a Gaussian derivative waveform, and an impedance of 50 Ohms.

Given a load impedance of $Z_a = R_a + iX_a$, a source impedance of $Z_s = R_s$, and an angular frequency of $\omega = 2\pi f$, the inductance and capacitance of the matching circuit components can be derived (see Appendix A) to be [66]

$$\mathcal{L} = \frac{\sqrt{R_a(R_s R_a^2 - R_s^2 R_a + X_a^2 R_s)} + X_a R_s}{\omega(R_a - R_s)}, \tag{7}$$

$$C = \sqrt{\frac{R_a}{\omega^2(R_s R_a^2 - R_s^2 R_a + X_a^2 R_s)}}. \tag{8}$$

The impedance of the best antenna was determined to be $Z_a = 311 - 197i$ Ohms at 300 MHz. Using Eqs. (7) and (8) produce an inductance $L = 87.8$ nH and a capacitance $C = 3.82$ pF for the circuit elements in Fig. 6.
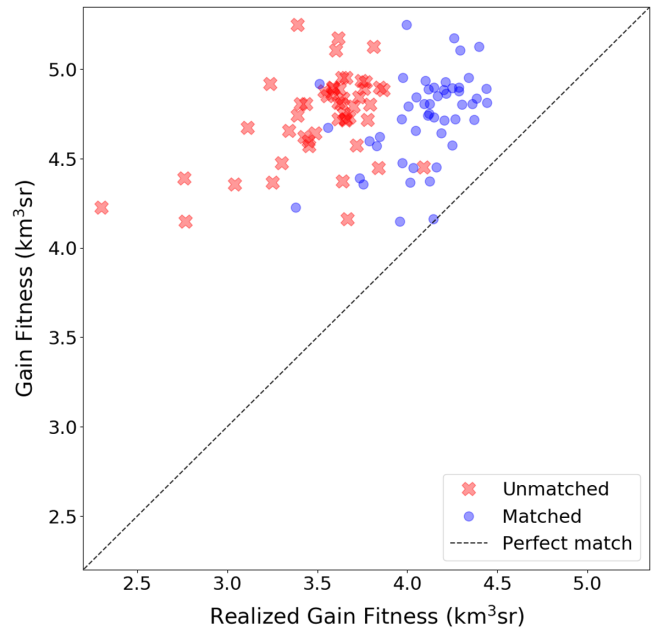

FIG. 7.   Fitness scores using gain vs realized gain with a matching circuit (blue circles) and without (red crosses).

The current ARA bicone achieves broadband matching to 50 Ω by putting four lines of its 200 Ω input impedance in parallel at the feed. Being part of the antenna design itself, this matching was naturally included in the simulation of the ARA bicones that we use to compare with our results, where we use the realized gains.

Figure 7 compares the fitness scores of the individuals from generation 23 when evaluated using the gain with perfect matching to the fitness scores when evaluated with
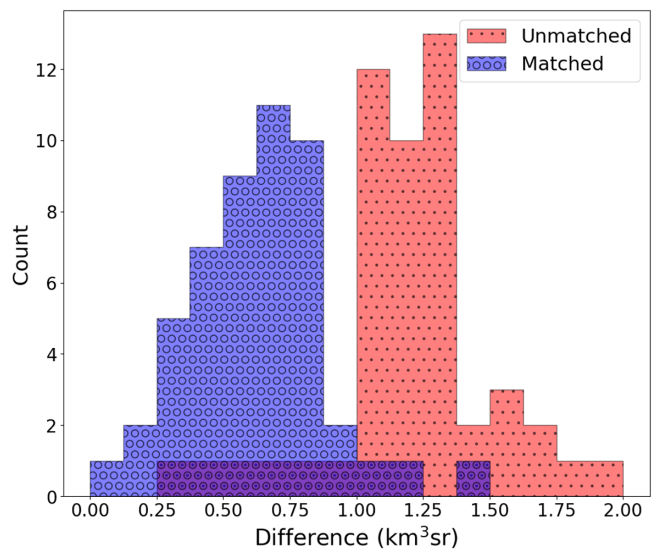

FIG. 8.   Antenna fitness score using perfect matching minus antenna fitness score using realized gain for unmatched (red/dots) and matched (blue/circles) antennas.

the realized gain. For the realized gain, we use a custom matching circuit for each individual designed as described above for 200 MHz. Naturally, the performance decreases when using realized gain; however, the matching circuit mitigates this effect.

Figure 8 shows a histogram of the fitness scores for each individual in generation 23 when calculated with gain assuming perfect matching minus the fitness scores of those individuals when calculated with realized gain for both the unmatched and matched cases. The unmatched and matched scores are, on average, 1.2 km^3 sr and 0.6 km^3 sr

lower than the scores evaluated with gain assuming perfect matching, respectively. The highest performing individual in generation 23 falls to 4.00 km^3 sr when evaluated with realized gain using the matching circuit. When applying the matching circuit, four antennas still exceeded the ARA bicone's score of 4.38 km^3 sr. Thus, there is still an improvement when comparing the realistic performance of evolved antennas with a matching circuit to the performance of the ARA antennas. We note that, in the future, the antennas will perform even better with a matching circuit that is broadband.
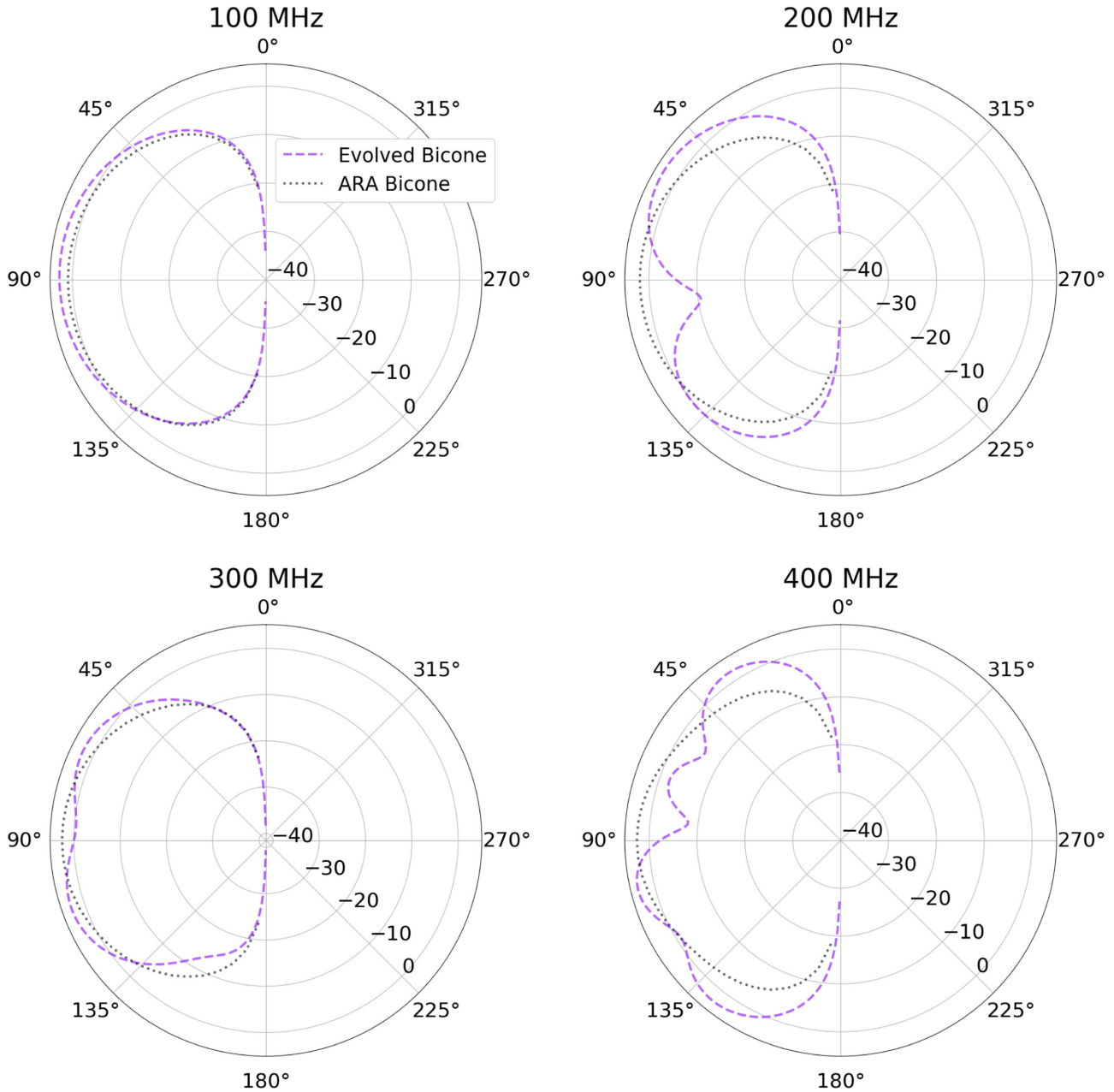
FIG. 9.   Antenna gain [Eq. (1)] for the evolved bicone (purple dashed line) and the ARA bicone (black dotted line) from XFdtd. Angles are measured from the positive vertical direction. See Appendix C for gain patterns for frequencies from 500 MHz to 1 GHz.
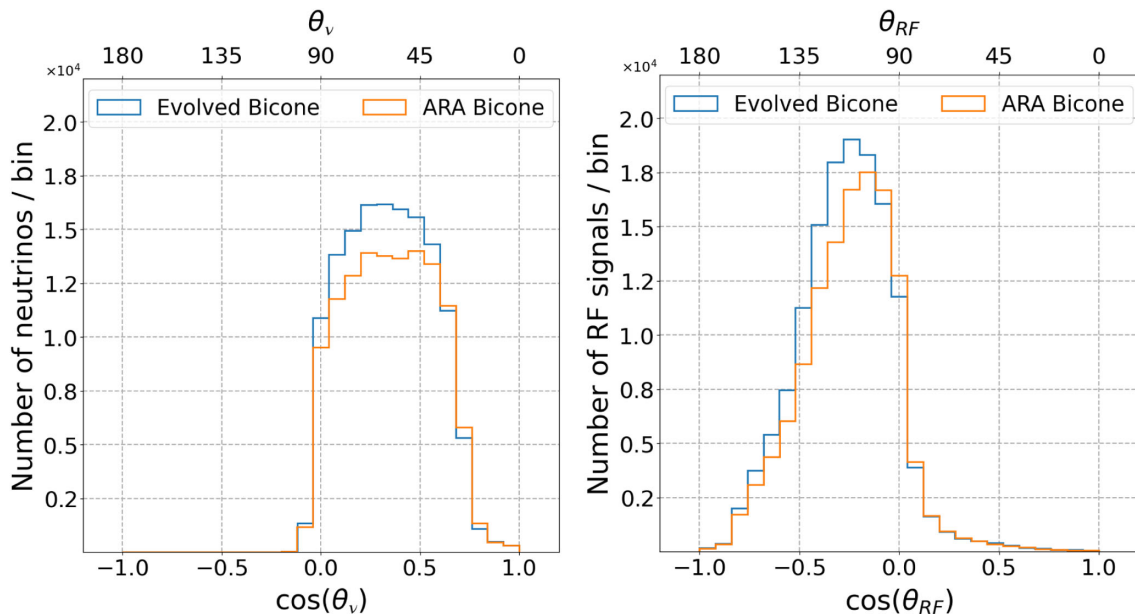
FIG. 10. Histograms of the number of detected neutrinos (left) and radio frequency (RF) signals (right) by each bicone for 3×10^7 simulated events. These angles denote the direction in which the event is seen by the detector, making them defined the same as the angles in Fig. 9. A RF angle of $\cos\theta_{\mathrm{RF}} > 0$ would mean that the signal is the incident from the above horizontal.

C. Physics interpretation of results

Here we interpret the previous results and investigate potential physical reasons for the observed behavior. It is important to determine what causes the improvement observed in fitness scores to validate the results of the GA. One notable difference between the antenna evolved here and the one used by ARA is the asymmetry of the geometry, which results in a qualitative difference in the shape of the antenna responses. In this section, we examine how the gain pattern of the evolved bicone compares to the ARA bicone at different frequencies, the distribution of incident angles of detected neutrinos, and how these results connect to the evolved asymmetrical bicone design.

Figure 9 shows the gain patterns of the best performing individual in the evolution, individual 8 in generation 23, compared to the gain pattern of the ARA Vpol antenna at four frequencies. The beam patterns show modestly higher peak gains (1–2 dB at low frequencies to a few dB at higher frequencies). While at 200 MHz the peak gain is actually at about 50° from the vertical, a preference for signals from below the surface becomes evident at higher frequencies, as can be seen in the 400 MHz gain pattern.

Figure 10 shows two histograms comparing the evolved bicone and the ARA bicone for a simulation with 3×10^7 neutrinos at 10^{18} eV. The left panel of Fig. 10 presents the number of detected neutrinos by ARA when the GENETIS antenna and existing ARA Vpol antenna are used, binned by the cosine of the zenith angle of the neutrino's originating direction, where $\cos\theta_\nu = 1$ ($\theta_\nu = 0°$) indicates that the neutrino originated from above the detector (down-going). Few events are detected by ARA with a cosine

angle less than about -0.2 (θ_ν more than about 100°) due to the absorption of those events in the Earth. When the GENETIS bicone is used, AraSim predicted 14% more detected events with neutrino incidents at angles between the horizontal and 37° below horizontal than with the current ARA design.

The right panel of Fig. 10 also shows the number of detected neutrinos, now binned by the cosine of the zenith angle at which the RF signal is the incident on the antenna. Here, $\cos\theta_{\mathrm{RF}} = -1$ ($\theta_{\mathrm{RF}} = 180°$) indicates that the radio
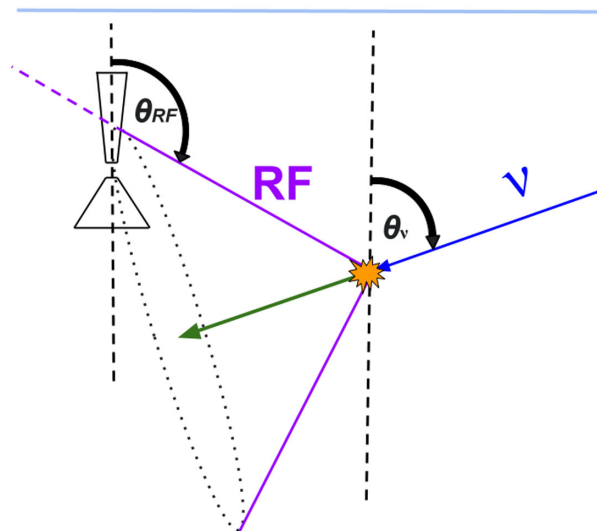

FIG. 11. A down-going neutrino interacting in the ice below the antenna, creating a particle cascade that produces Askaryan radiation that is viewed by the antenna.

signal is the incident from below. ARA with the evolved bicone is predicted to detect more RF signals between cosine angles of −0.2 and −0.6 (about 100–130° from the vertical), meaning more signals were detected at angles originating from events below horizontal. These results are consistent with an improvement in the detection of down-going neutrinos that interact in the ice and produce radio signals that propagate up to the detectors. This is shown in Fig. 11, where a down-going neutrino interacts in the ice and creates a particle cascade.

We can see here that improvements in the antenna gain pattern for signals from the upward direction seen in Fig. 9 do not produce a strong contribution to the improved performance of the antenna for detecting neutrinos. This is because for those events the radio signal would arrive from above the horizon, and those events only account for about 10% of detected events, as shown on the right side of Fig. 10.

VII. CONCLUSION

With these results, GENETIS presents the results of a GA-designed antenna using a physics outcome as a measure of fitness and lays the foundation for future detector optimizations. We show that a GA evolving six parameters of a bicone antenna can evolve a design that results in an ARA detector with an 11% greater sensitivity to in-ice UHE neutrino detection than one using the current Vpol antennas. The improved design outperforms the existing ARA Vpol antenna in detecting down-going neutrinos that produce radio waves that propagate up towards the detector.

VIII. FUTURE WORK

An antenna prototype of the best performing individual will be fabricated through additive manufacturing using industrial 3D printers capable of processing metals at The Ohio State University Center for Design and Manufacturing Excellence. This will allow us to compare laboratory measurements to the results of the simulations produced by GENETIS and therefore validate the optimization process. In future work, we will continue to evolve improved antennas with the goal of doubling the current ARA Vpol antenna sensitivity. If an evolved antenna successfully improves on the current Vpol antennas by a factor of 2, it will be deployed in-ice for further testing.

GENETIS plans to improve on this work to broaden the parameter space while ensuring that results remain robust. In general, as the parameter space is increased it will take more generations for the GA to converge. More individuals can ensure that the breadth of the parameter space is covered and help to prevent an early convergence of the results. Additionally, in the future, we will simulate with a predicted neutrino energy spectrum instead of using a single energy. Decreasing the angle step size of the gain

pattern simulations would also provide a more accurate result.

The GENETIS Collaboration is currently working on several improvements to the GA to further improve computational efficiency, convergence speed, and maximum fitness. First, we are introducing more complex antenna geometries, such as bicones with nonlinear sides. These antennas would require additional genes that describe the coefficients of polynomials that represent the shape of the sides of the bicone. This project is underway, and the evolution of other types of antennas will soon begin development, including the optimization of the Hpol antennas and comparing the performance of the evolved designs to the current ARA Hpol antenna. In the future, we will be testing the effect of the borehole size on the evolved fitness scores. We are also exploring the use of additional and more advanced selection methods and genetic operations, including rank selection and elitism.

Additionally, we will continue to refine our work flow to improve the sophistication of our modeling, such as by constructing broadband matching circuits for evolved antennas. The construction of a single frequency matching circuit can currently be automated in the loop, allowing us to evolve using realized gain directly. We plan to fully implement this with broadband matching circuits to more realistically and efficiently evolve designs.

In the future, the GENETIS project will expand beyond antenna design and explore other aspects of experimental design and analysis, including detector layouts and trigger optimization. As a first step toward this goal, we will develop the capability to evolve the layout of an array of antenna stations for UHE detection together with the antenna designs. The GENETIS project will also expand to employ different types of computational intelligence and machine learning techniques and perform optimizations for other experimental applications.

The successful deployment of GA-designed detectors could pave the way for additional applications of optimization heuristics for the design of scientific instruments. Expanded research in this area will streamline the optimization of the design of many types of experiments across fields for superior science outcomes.

APPENDIX A: IMPEDANCE MATCHING

The following is a derivation of Eqs. (7) and (8) for the elements of a single frequency matching circuit. We begin with a source resistor with impedance $Z_s = R_s$ and a load (antenna) impedance $Z_a = R_a + iX_a$.

In summary, we seek to use purely reactive circuit components to minimize reflection and deliver all of the power from the source to the load. To do this, we will first construct a parallel subcircuit (the parallel inductor-load resistor in Fig. 6), which has a resistance equal to the resistance of the source resistor. In this case, the parallel component will be an inductor.

This parallel subcircuit has impedance

$$Z_p = R_p + iX_p = \left(\frac{1}{R_a + iX_a} + \frac{1}{i\omega\mathcal{L}} \right)^{-1}, \quad \text{(A1)}$$

where $i\omega L$ is the impedance of the inductor. We want to find an inductance such that $R_p = R_s$. We can rearrange Eq. (A1) to solve for the impedance of the inductor:

$$i\omega\mathcal{L} = \frac{R_p R_a - X_p X_a + i(X_p R_a + R_p X_a)}{R_a - R_p + i(X_a - X_p)}. \quad \text{(A2)}$$

Equation (A2) gives the unknown L in terms of another unknown X_p. To simplify, we can rewrite it as

$$i\omega\mathcal{L} = \frac{A + iB}{C + iD}, \quad \text{(A3)}$$

using the substitutions

$$A = R_p R_a - X_p X_a$$
$$B = X_p R_a + R_p X_a$$
$$C = R_a - R_p$$
$$D = X_a - X_p.$$

We can further rewrite Eq. (A3) so that the denominator is purely real:

$$i\omega\mathcal{L} = \frac{AC + BD + i(BC - AD)}{C^2 + D^2}. \quad \text{(A4)}$$

Since the impedance of the inductor must be purely reactive (imaginary), we obtain a second equation to constrain our two unknowns: $AC + BD = 0$. We substitute $D = -AC/B$ into Eq. (A4) to obtain

$$i\omega\mathcal{L} = \frac{iB}{C}. \quad \text{(A5)}$$

Using the condition $D = -\frac{AC}{B}$, we can solve for X_p:

$$X_p = \sqrt{\frac{R_p R_a^2 + X_a^2 R_p - R_a R_p^2}{R_a}}. \quad \text{(A6)}$$

Finally, using Eq. (A6) in B, substituting B and C back into Eq. (A5), setting $R_p = R_s$, and solving for L yields Eq. (7).

Using an inductor with inductance given by Eq. (7) gives a parallel subcircuit with $Z_p = R_p + iX_p = R_s + iX_p$. Now, we will use a capacitor to offset the reactive component of Z_p so that $Z = Z_p + Z_c = R_s$. This gives us

$$Z = Z_p + Z_c = R_s + iX_p + R_c + iX_c. \quad \text{(A7)}$$

Since Z should be purely real, the reactance of the capacitor is given by

$$X_c = -X_p. \quad \text{(A8)}$$

The reactance of a capacitor is $X_c = \frac{1}{\omega C}$, so Eq. (A8) gives us

$$C = \frac{1}{\omega X_p}. \quad \text{(A9)}$$

Note that the capacitance is negative here. The negative sign indicates that the capacitor serves to *decrease* the circuit's reactance. Substituting X_p from Eq. (A6) into Eq. (A9) yields Eq. (8).

This process of impedance matching can be visualized using a Smith chart [67]. Figure 12 [68] is a Smith chart showing a load impedance Z_L and a source impedance Z_0. The purple path connecting Z_L to A represents the shunt inductor we designed. The inductor in parallel with the load
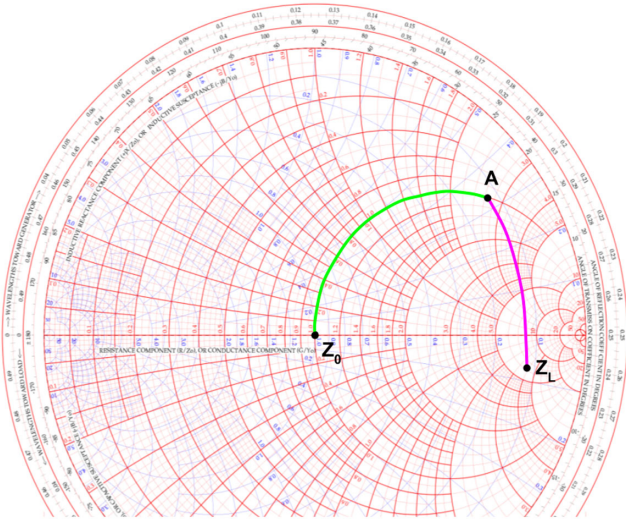
FIG. 12.   Smith chart example matching load Z_L to source Z_0 [68].

forms a subcircuit with a resistance equal to the resistance of the source, represented by the red circle passing through Z_0 and A. The series capacitor, represented by the green path, moves us along the red circle by changing the circuit's reactance until it matches the reactance of Z_0.

APPENDIX B: OPTIMIZATION OF THE GA

The parameter values of the GENETIS GA used in this work were chosen by optimizing the performance of a test GA, which utilized a faster and simpler fitness function. Besides the fitness function, the test GA is identical to the GA used in the GENETIS loop. This allowed many variations of the GA parameter values to be tested in a short amount of time. The test GA does not optimize antenna designs to improve their performance in a physics experiment. Instead, it optimizes the parameters of the GA itself, such as the fraction of individuals formed through crossover, reproduction, and injection. This effectively means that we are evolving the same antenna genes but with a simpler fitness score that requires no simulation. Due to the stochastic nature of GAs, each evolution with a given set of GA parameters was repeated 10 times and the average maximum fitness score of those ten runs was used as the measure of the GA's performance given those GA parameters. This was used to determine which parameters to use for the GENETIS GA.

The test GA uses a fitness score based on the antenna geometry compared to a target geometry fitness score to evaluate an antenna's performance instead of results from computationally expensive simulations. To do this, a single bicone antenna was selected as the "reference" antenna. The test GA generates populations in the same manner as discussed in Secs. V A and V C. However, the antenna's fitness score is calculated by measuring how similar it is to

the reference antenna. The fitness score of an antenna is given by

$$F_i = 100 - \sum |R_i - g_i|. \tag{B1}$$

Here, F_i is the individual's fitness score, R_i is the value of the ith gene of the reference antenna, and g_i is the value of the ith gene of the individual. Since the objective of the test GA is to evolve to an antenna that is identical to the reference antenna, the maximum fitness score is 100.

Because the fitness score is determined by an equation instead of simulations, a single generation can be generated and evaluated in less than 1 second. This allows a run of 100 generations to be executed in less than 2 minutes, making it computationally inexpensive to evaluate the performance over a wide range of possible parameters.

The testing procedures are highlighted in more depth below. We held the parent selection methods constant, given by results from a preliminary test. We then varied the number of individuals generated through crossover, repro- duction, and injection operators. Here, the fraction of individuals generated through crossover was varied from 60% to 80% in step sizes of 10%. The fraction of individuals generated through reproduction varied from 2% to 20% in step sizes of 2%. The remaining individuals were generated using the injection operator (from 0% to 38% in step sizes of 2%). This test was run using 100 individuals in each generation over 30 generations and was repeated 10 times for each combination of parameters.

The results of this optimization are presented in Fig. 13. Each pair of red and blue bars represents the performance of the test GA for the associated parameters, with the blue bars representing the average of the highest fitness scores achieved by each of the ten runs and the red bars representing the absolute highest fitness score achieved by any the ten runs. The GENETIS GA discussed in this paper used the same ratio of operators to generate new individuals as the run in this test with the highest average maximum fitness score (rounded to align with a population of 50 individuals rather than 100).

In addition to evaluating the optimal combination of generative operators, the test GA was also used to test the impact of the population size on performance. In this test, the test GA was run 10 times for 30 generations with population sizes of 50, 100, and 1000 individuals per generation. The results are shown in Fig. 14. Note that the fitness score used for this test was adjusted to vary from 0 to 1.

As expected, the performance of the GA improves with larger population sizes. However, the increase in perfor- mance grows logarithmically with population size. Because of the linear increase in computational expense with population size, a population size of 50 individuals is justified as an efficient population size.
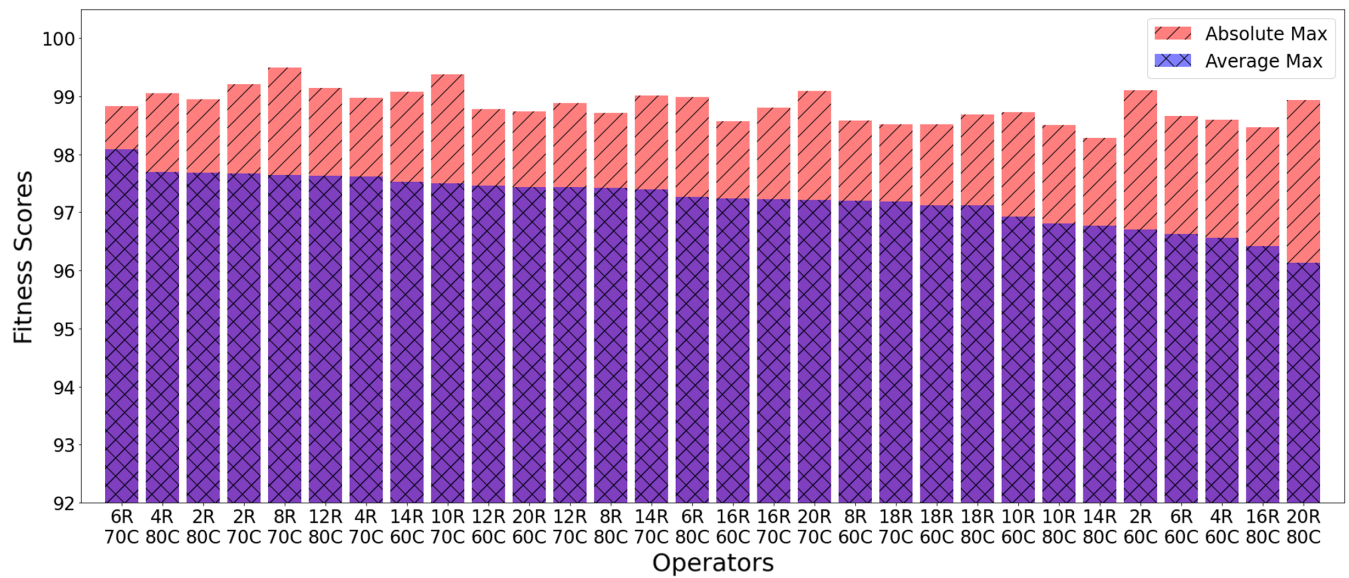
FIG. 13. Overlapping bar plot of results from running the test GA with various combinations of generative operator ratios. The labels on the x axis indicate the percent of individuals formed through reproduction ("R") and crossover ("C"), with the remainder coming from injection. The results are arranged in descending order of performance as measured by the average maximum score (purple/crosses) of ten runs using the labeled set of ratios. Note that the zero has been suppressed on this plot. While there is no guarantee that the maximum score of a run is close to 100, no individual run in this test produced a maximum fitness score below 92.
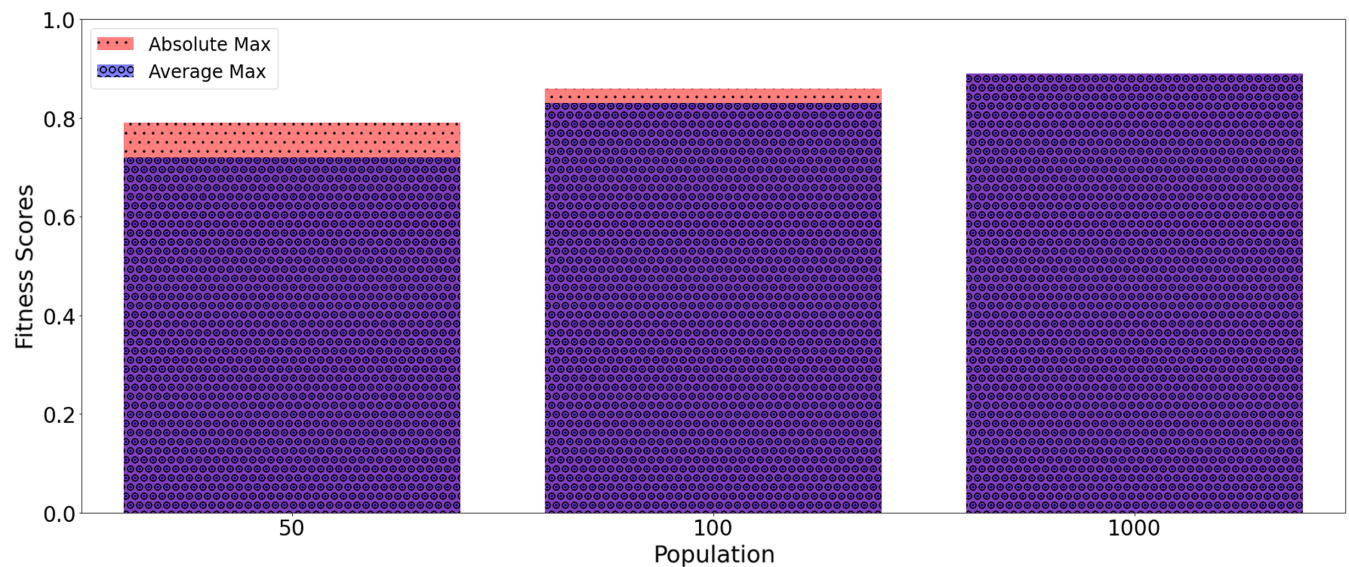

FIG. 14. Overlapping bar chart showing the performance of the test GA for different population sizes. For this study the fitness score was adjusted to range from 0 to 1.

APPENDIX C: ADDITIONAL GAIN PATTERNS

In addition to those in Fig. 9 in Sec. VI, we have included additional gain patterns for the ARA and evolved bicones up to 1 GHz in Figs. 15 and 16.
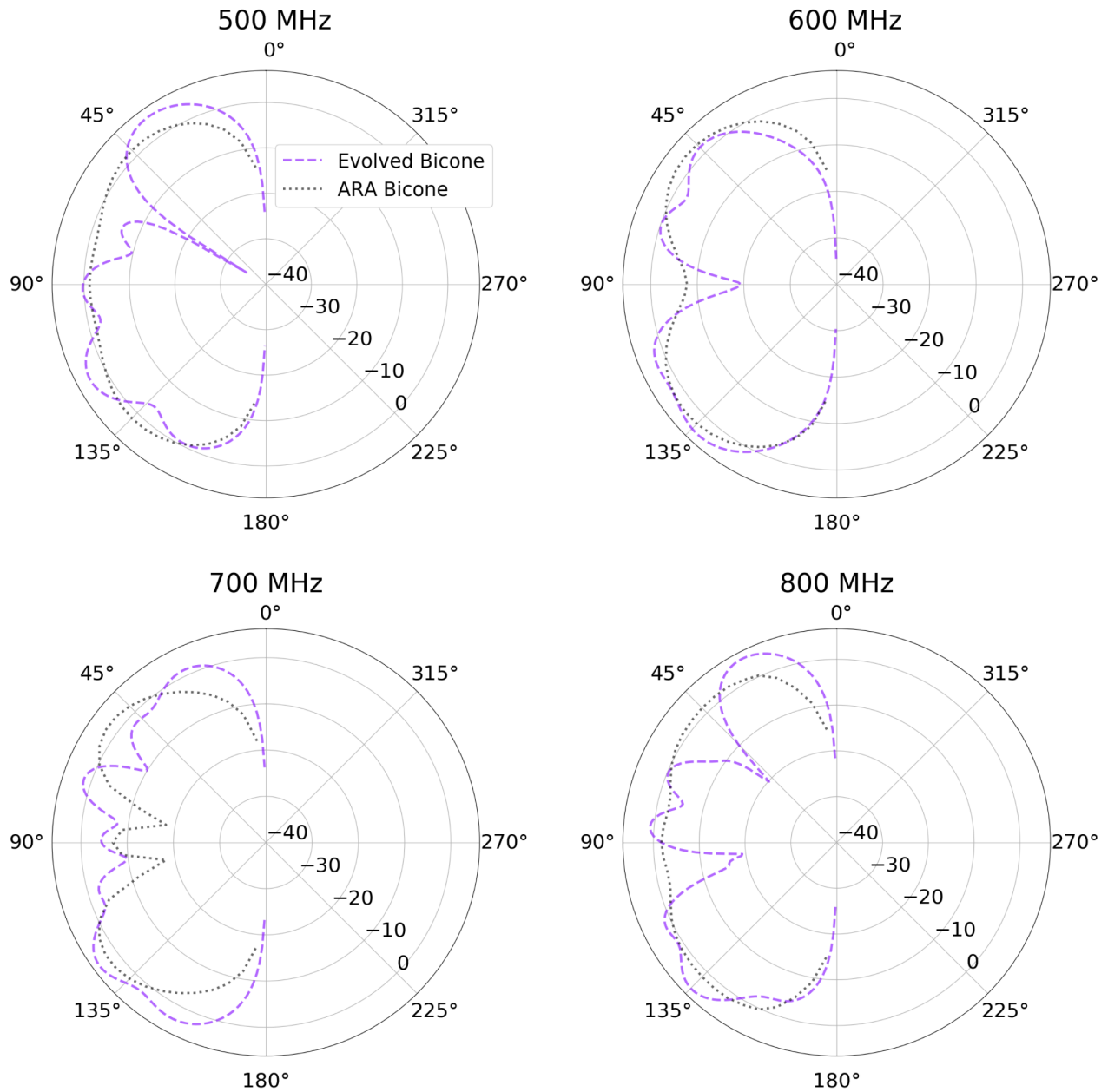

FIG. 15.   Gain patterns for the evolved and ARA bicones at 500–800 MHz.
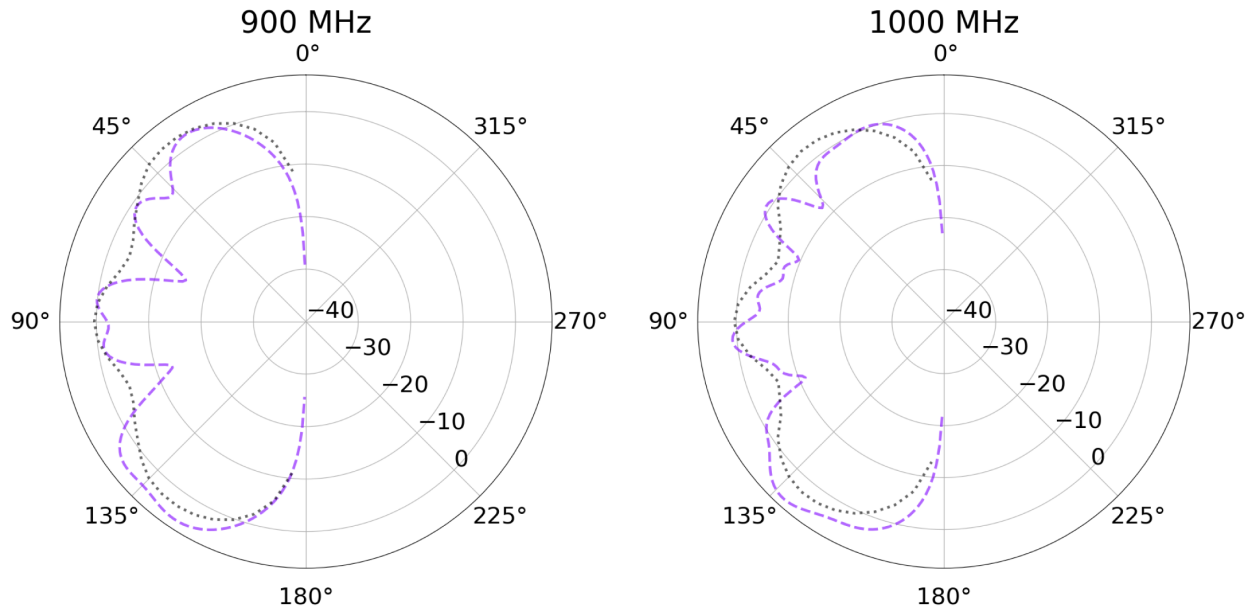
FIG. 16.   Gain patterns for the evolved and ARA bicones at 900 and 1000 MHz.

APPENDIX D: COMPARISON WITH EVOLUTION OF SYMMETRIC ANTENNAS

In the interest of comparison, an evolution was run using the same GA but holding the genes of the top and bottom antenna to be equivalent, making a symmetric bicone. The results of the evolution can be seen in the violin plot in Fig. 17. Compared to the evolution of the asymmetric antennas, this evolution shows a mean and median that remain relatively flat over the 31 generations and close to the ARA Vpol score.
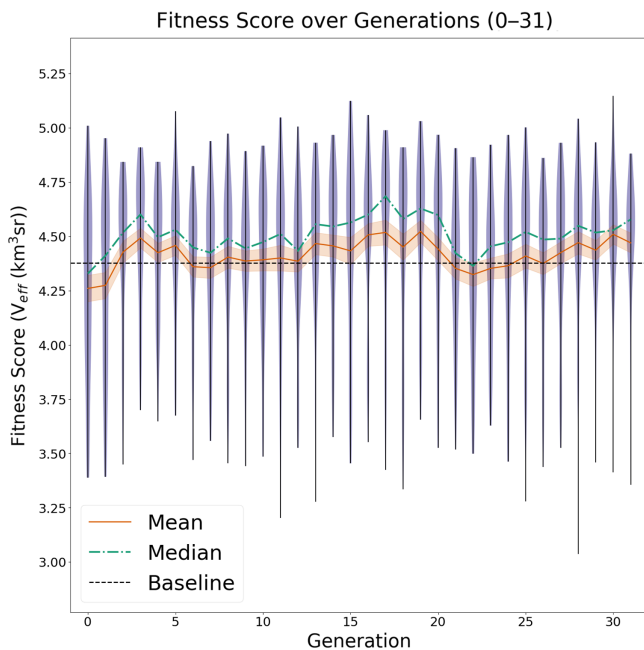
The highest scoring individual from the symmetric run was individual 3 in generation 30, with a fitness score calculated during the run of 5.15 ± 0.2 km^3 sr, compared to 5.25 ± 0.2 km^3 sr for the top individual from the evolution of asymmetric antennas. After simulating the top five individuals from the run again using 3×10^7 neutrinos, the best individual remained the best performing, with a score of 4.78 ± 0.02 km^3 sr, compared to 4.90 ± 0.02 km^3 sr from the resimulation of the best individual from the evolution of asymmetric antennas, showing that

FIG. 17.   Results of the GA for the symmetric evolution.
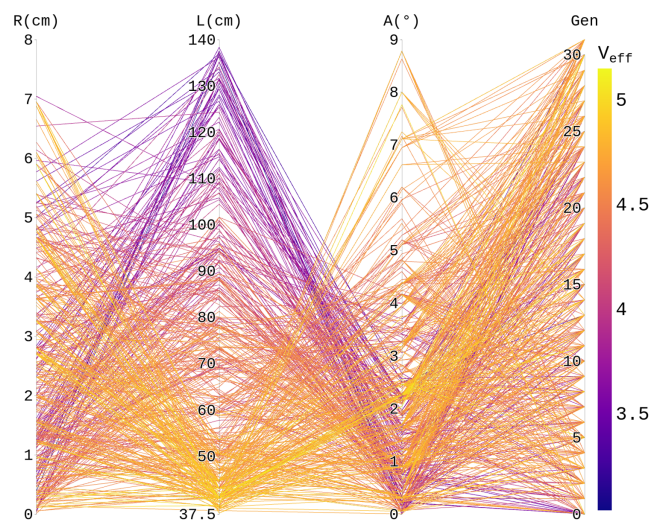

FIG. 18.   A parallel coordinate plot of the genes in the symmetric evolution.

the improved fitness score from the evolution of asymmetric antennas was significant. The best individual from the evolution of the symmetric antennas had a 9% higher fitness score than the ARA Vpol antenna, compared to the 11% higher fitness score for the best individual from evolution of asymmetric antennas. None of the resimulated scores of the top five individuals from the evolution of symmetric antennas had a higher fitness score than any of the resimulated top five individuals from the evolution of asymmetric antennas.

The parallel coordinate plot in Fig. 18 illustrates the genes and fitness scores for each individual in the evolution of symmetric antennas. Antennas with shorter lengths performed best, which agrees with the results for the bottom cone of the antennas in the evolution of asymmetric antennas. This is also shown in Table III, which shows the

TABLE III. Genes and resimulated fitness scores of the five best individuals from the evolution of the symmetric antennas.

Radius (cm)	Length (cm)	Angle (°)	Score (km^3 sr)
5.9	41.7	2.0	4.78 ± 0.01
1.6	41.0	2.3	4.62 ± 0.01
0.97	40.0	2.5	4.73 ± 0.01
2.8	41.1	2.3	4.75 ± 0.01
1.9	41.1	1.8	4.75 ± 0.01

genes of the top five individuals from the evolution of symmetric antennas. All of the top five individuals had a length between 40 cm and 42 cm. The top five individuals in the evolution of asymmetric antennas all had lengths of approximately 45 cm.

[1] J. Frenzel, IEEE Potentials **12,** 21 (1993).
[2] M. M. Raghuwanshi and O. Kakde, in *Proceedings of the 8th Asia Pacific symposium on intelligent and evolutionary systems* (2004), Vol. 11.
[3] G. Hornby *et al.*, American Institute of Aeronautics and Astronautics (2006), https://ti.arc.nasa.gov/m/pub-archive/1244h/1244(Hornby).pdf.
[4] E. Jones and W. Joines, IEEE Trans. Antennas Propag. **45,** 1386 (1997).
[5] A. Boag, A. Boag, E. Michielssen, and R. Mittra, IEEE Trans. Antennas Propag. **44** (1996).
[6] J. Deng, X. Chen, R. Yu, and X. Wen, in *2014 International Workshop on Antenna Technology: Small Antennas, Novel EM Structures and Materials, and Applications (iWAT)* (2014), pp. 308–309, https://ieeexplore.ieee.org/document/6958672.
[7] M. Gulati, S. Siddhartha, Y. Vedi, and M. Susila, in *2018 International Conference on Wireless Communications, Signal Processing and Networking (WiSPNET)* (2018), pp. 1–2, https://ieeexplore.ieee.org/document/8538585.
[8] R. Deepika, P. Manikandan, and P. Sivakumar, in *2017 IEEE International Conference on Electrical, Instrumentation and Communication Engineering (ICEICE)* (2017), p. 1, https://ieeexplore.ieee.org/document/8191862.
[9] L. Xie, Y. Jiao, G. Wei, G. Zhao, and F. Zhang, Microwave Opt. Technol. Lett. **53,** 2135 (2011).
[10] R. Lovestead and A. Safaai-Jazi, Microwave Opt. Technol. Lett. **62,** 425 (2020).
[11] D. Eclercy, A. Reineix, and B. Jecko, Microwave Opt. Technol. Lett. **16,** 72 (1998).
[12] R. Haupt, IEEE Trans. Antennas Propag. **52,** 1976 (2004).
[13] C. Laohapensaeng and C. Free, in *Asia Pacific Microwave Conference-Proceedings* (2005), Vol. 62, pp. 425–431.
[14] R. L. Haupt, IEEE Trans. Antennas Propag. **55,** 577 (2007).
[15] B. Liu, H. Hu, H. Han, H. Lv, and L. Li, Nucl. Instrum. Methods Phys. Res., Sect. A **897,** 54 (2018).
[16] A. Liu, A. Bross, and D. Neuffer, Nucl. Instrum. Methods Phys. Res., Sect. A **794,** 200 (2015).
[17] D. McCarthy, N. Trappe, J. A. Murphy, C. O'Sullivan, M. Gradziel, S. Doherty, P. G. Huggard, A. Polegro, and M. van der Vorst, Infrared Phys. Technol. **76,** 32 (2016).
[18] M. Calviani, S. D. Luise, V. Galymov, and P. Velten, Nucl. Part. Phys. Proc. **273–275,** 2681 (2016).
[19] H. Schellman, in *The 39th International Conference on High Energy Physics* (2018), Vol. 340.
[20] A. G. Baydin *et al.* (MODE Collaboration), Nucl. Phys. News **31,** 25 (2021).
[21] D. Kastanya, Ann. Nucl. Energy **46,** 160 (2012).
[22] E. B. Flynn and M. D. Todd, J. Intell. Mater. Syst. Struct. **21,** 265 (2010).
[23] N. Kleedtke, M. Hua, and S. Pozzi, Nucl. Instrum. Methods Phys. Res., Sect. A **988** (2021).
[24] S. Abdullin, Nucl. Instrum. Methods Phys. Res., Sect. A **502,** 693 (2003).
[25] J. H. Holland, *Adaptation in Natural and Artificial Systems* (University of Michigan Press, Ann Arbor, MI, 1975), second edition, 1992.
[26] L. Davis, *Handbook of Genetic Algorithms* (Van Nostrand Reinhold, New York, 2016).
[27] D. Goldberg, *Genetic Algorithms in Search, Optimization and Machine Learning*, 1st ed. (Addison-Wesley Longman Publishing Co., Inc., USA, 1989).
[28] R. Zebulum *et al.*, *Evolutionary Electronics* (CRC Press, Boca Raton, 2018).
[29] A. Shuckla *et al.*, in *2015 International Conference on Futuristic Trends on Computational Analysis and Knowledge Management* (2015).
[30] R. Haupt and S. Haupt, *Practical Genetic Algorithms* (John Wiley & Sons, Inc, New York, 1998).

[31] D. Beasley, D. R. Bull, and R. R. Martin, Univ. Comput. **15,** 56 (1993).

[32] D. Fogel, IEEE Trans. Neural Networks **5**, 3 (1994).

[33] K. Man, K. Tang, and S. Kwong, IEEE Trans. Ind. Electron. **43**, 519 (1996).

[34] J. Zhang, Z.-h. Zhan, Y. Lin, N. Chen, Y.-j. Gong, J.-h. Zhong, H. S. Chung, Y. Li, and Y.-h. Shi, IEEE Comput. Intell. Mag. **6**, 68 (2011).

[35] T.-P. Hong, H.-S. Wang, W.-Y. Lin, and W.-Y. Lee, Appl. Intell. **16**, 7 (2002).

[36] M. G. Aartsen *et al.* (IceCube Collaboration), Phys. Rev. Lett. **115**, 081102 (2015).

[37] I. Kravchenko, Phys. Rev. D **73**, 082002 (2006).

[38] P. Allison *et al.*, arXiv:1912.00987.

[39] P. Allison *et al.*, Astropart. Phys. **70**, 62 (2015).

[40] P. Gorham *et al.*, Phys. Rev. D **99** (2019).

[41] A. Connolly, R. S. Thorne, and D. Waters, Phys. Rev. D **83**, 113009 (2011).

[42] R. Gandhi, C. Quigg, M. Hall Reno, and I. Sarcevic, Astropart. Phys. **5**, 81 (1996).

[43] G. Askaryan, J. Phys. Soc. Jpn. **17**, 257 (1962).

[44] T. Heuge and D. Besson, Prog. Theor. Exp. Phys. **2017**, 12A106 (2017).

[45] A. Connolly and A. Vieregg, arXiv:1607.08232.

[46] Q. Abarr *et al.*, J. Instrum. **16**, P08035 (2021).

[47] P. Allison *et al.* (ARA Collaboration), Phys. Rev. D **93**, 082003 (2016).

[48] A. Anker *et al.*, Adv. Space Res. **64**, 2595 (2019).

[49] J. Aguilar *et al.*, arXiv:1907.12526.

[50] P. Allison *et al.*, arXiv:1907.11125.

[51] S. Archambault *et al.*, in *35th International Cosmic Ray Conference* (2017).

[52] P. Allison *et al.*, Astropart. Phys. **35**, 457 (2012).

[53] K. Hoffman *et al.*, in *33rd International Cosmic Ray Conference* (2013).

[54] J. Aguilar *et al.*, J. Instrum. **16**, P03025 (2021).

[55] R. Luebbers, in *2006 IEEE Antennas and Propagation Society International Symposium* (2006), pp. 119–122, 10.1109/APS.2006.1710467.

[56] Remcom (private communication).

[57] *IEEE Standard for Definitions of Terms for Antennas* (IEEE, 2014), 10.1109/IEEESTD.2014.6758443.

[58] *IEEE Standard Test Procedures for Antennas* (IEEE, 1979), 10.1109/IEEESTD.1979.120310.

[59] P. Allison *et al.*, Astropart. Phys. **108**, 63 (2019).

[60] A. Lipowski and D. Lipowska, Physica (Amsterdam) **391A**, 2193 (2012).

[61] J. Zhong, X. Hu, M. Gu, and J. Zhang, in *International Conference on Computational Intelligence for Modelling, Control and Automation and International Conference on Intelligent Agents, Web Technologies and Internet Commerce (CIMCA-IAWTIC'06)* (2005), pp. 1115–1121.

[62] G. Syswerda, in *Proceedings of the 3rd International Conference on Genetic Algorithms* (1989), pp. 2–9.

[63] M. Moed, C. Stewart, and R. Kelly, in *1991 Third International Conference on Tools for Artificial Intelligence* (IEEE Computer Society, Los Alamitos, CA, USA, 1991), pp. 500–501.

[64] L. W. Nagel and D. Pederson, SPICE (Simulation Program with Integrated Circuit Emphasis), Technical Report UCB/ERL M382, EECS Department, University of California, Berkeley, 1973.

[65] C. Glaser *et al.*, Eur. Phys. J. C **80**, 77 (2020).

[66] A. M. Niknejad, *Electromagnetics for High-Speed Analog and Digital Communication Circuits* (Cambridge University Press, Cambridge, England, 2007).

[67] F. Caspers, arXiv:1201.4068.

[68] J. Rolla, Applications of evolutionary algorithms in ultra-high energy neutrino astrophysics [Currently unpublished Ph.D. thesis], Ph.D. thesis, The Ohio State University, 2021.